Dayside magnetopause reconnection and flux transfer events: BepiColombo earth-Flyby observations

Weijie Sun[1], James A. Slavin[1], Rumi Nakamura[2], Daniel Heyner[3], Karlheinz J. Trattner[4], Johannes Z. D. Mieth[3], Jiutong Zhao[5], Qiu-Gang Zong[5], Sae Aizawa[6,7], Nicolas Andre[6], Yoshifumi Saito[8]

[1]Department of Climate and Space Sciences and Engineering, University of Michigan, Ann Arbor, MI 48109, United States
[2]Space Research Institute, Austrian Academy of Sciences, Schmiedlstraße 6, 8042 Graz, Austria
[3]Institut für Geophysik und extraterrestrische Physik, Technische Universität Braunschweig, 38106 Braunschweig, Germany
[4]Laboratory for Atmospheric and Space Physics, University of Colorado, Boulder, CO 80303, USA
[5]School of Earth and Space Sciences, Peking University, Beijing 100871, China
[6]Institut de Recherche en Astrophysique et Planétologie, CNRS-UPS-CNES, Toulouse, France
[7]Department of Geophysics, Graduate School of Science, Tohoku University, Sendai, Japan
[8]Japan Aerospace Exploration Agency, Institute of Space and Astronautical Science, Kanagawa, Japan

Correspondence to: Weijie Sun (wjsun@umich.edu)

Abstract. This study analyzes the flux transfer event (FTE)-type flux ropes and magnetic reconnection around the dayside magnetopause during BepiColombo's Earth flyby. The magnetosheath has a high plasma β (~ 8) and the IMF has a significant radial component. Six flux ropes are identified. The motion of flux ropes together with the maximum magnetic shear model suggest that the reconnection X-line swipes BepiColombo near the magnetic equator due to an increase of the radial IMF. The flux rope with the highest flux content contains a clear coalescence signature, i.e., two smaller flux ropes merging, supporting theoretical predictions the flux content of flux ropes can grow through coalescence. The coalescence of the two FTE-type flux ropes takes place through secondary reconnection at the point of contact between the two flux ropes. The BepiColombo measurements indicate that a large normalized guide field and a reconnection rate comparable to that measured at the magnetopause (~ 0.1).

1. Introduction

Flux transfer events (FTEs) are frequently observed near the outer boundaries, i.e., magnetopause, of planetary magnetospheres, including on the Earth (e.g., Russell and Elphic, 1978; Saunders et al., 1984; Wang et al., 2005), Mercury (Russell and Walker, 1985; Slavin et al., 2009; 2010; 2012; Imber et al., 2014; Sun et al., 2020), Saturn (Jasinski et al., 2016; 2021) and Jupiter (Walker and Russell, 1985; Lai et al., 2012). Some of the FTEs have magnetic flux ropes at their cores, which consist of helical magnetic field lines surrounding stronger magnetic fields paralleling their central axes (Paschmann et al., 1982; Lee et al., 1993). These FTE-type flux ropes are created by multiple X-line reconnections in the magnetopause during intervals of significant magnetic shear across this current sheet (Lee and Fu, 1985; Raeder, 2006). As a result, the FTE-type flux ropes signal not only the occurrence of magnetic reconnection but their direction of travel can be used to infer the relative location of the reconnection X-lines at the magnetopause.

The FTEs usually include magnetic field lines with one end connecting to the solar wind and the other to the cusp. They contribute to the transport of magnetic flux from the dayside to the nightside magnetosphere that drives the Dungey cycle in dipolar planetary magnetospheres. Sun et al. (2022) has recently reviewed the contributions of FTE-type flux ropes to the Dungey cycle in dipolar planetary magnetospheres. In Mercury's magnetosphere, the FTE-type flux ropes transport majority (>60%) of the circulated flux (Slavin et al., 2010; Imber et al., 2014; Sun et al., 2020). In contrast, FTE-type flux ropes are estimated to transport only a small portion (<5%) of the circulated flux at Earth (Lockwood et al., 1995; Fear et al., 2017). And for the giant outer planetary magnetospheres at Jupiter and Saturn, they appear to transport a negligible magnetic flux (< 1%) for the solar wind-driven portion of their internal convection (Jasinski et al., 2021).

The FTEs on Earth's magnetosphere appear most frequently during periods of the southward interplanetary magnetic field (IMF) when the magnetic shear angle across the magnetopause is larger than 90° (e.g., Rijnbeek et al., 1984; Kuo et al., 1995; Wang et al., 2006). The locations of magnetopause X-lines are closely related to the orientation of the IMF. For example, during the purely southward IMF, reconnection most likely occurs on the magnetopause near the subsolar point (Dungey, 1961). During the purely northward IMF, reconnections occur on the magnetopause tailward of the cusp (Dungey, 1961; Song and Russell, 1992; Shi et al., 2009; 2013; Gou et al., 2016). Magnetic reconnection is also thought to occur at the dayside magnetopause under the strong radial IMF (B_x dominate) (Belenkaya, 1998; Luhmann et al., 1984; Pi et al., 2017; Tang et al., 2013; Toledo-Redondo et al., 2021), but the strong radial IMF conditions are less well studied.

Coalescence, which refers to the merging of neighboring flux ropes, is thought to be an important process in space plasma physics (Biskamp and Welter, 1980; Dorelli and Bhattacharjee, 2009; Fermo et al., 2011; Hoilijoki et al., 2017). The merging of flux ropes is associated with secondary reconnection, and changes in magnetic field configuration caused by this secondary reconnection can energize particles, especially electrons (Drake et al., 2006). Furthermore, several studies have suggested that FTE-type flux ropes are initially formed at electron to ion scales. They then grow through coalescence, thereby, increasing their magnetic flux content (Fermo et al., 2011; Akhavan-Tafti et al., 2018). **NASA's Magnetospheric Multiscale (MMS) Mission (Burch et al., 2016) has provided several observations of secondary reconnections between neighboring flux ropes (see, Zhou et al., 2017), between the flux rope and Earth's dipole magnetic field (Poh et al., 2019), and between interlinked flux tubes (Øieroset et al., 2016; Kacem et al., 2018).**

This study investigates FTE-type flux ropes and reconnection at the Earth's dayside magnetopause during BepiColombo's flyby on 10 April 2020. The paper is arranged as follows. Section 2 introduces the BepiColombo mission and the measurements during Earth's dayside magnetopause crossing. Section 3 analyzes the distribution of magnetopause reconnection with a strong radial IMF component, and the properties of the flux ropes, including a coalescence event. Section 4 provides a summary of our results.

2. BepiColombo Dayside Magnetopause Crossing

2.1. Spacecraft and Instrumentation

BepiColombo, which is a joint mission by the ESA and the JAXA, consists of two spacecraft, which are the Mercury Planetary Orbiter (MPO) and Mercury Magnetospheric Orbiter (MMO, or Mio). These spacecraft together will carry out detailed investigations of Mercury's interior, surface, exosphere, and magnetosphere (Milillo et al., 2020; Murakami et al., 2020; Benkhoff et al., 2010). The mission made its first planetary flyby maneuver at the Earth on 10 April 2020 (Mangano et al., 2021), during which several instruments collected measurements. **The MPO and the MMO were attached during the Earth flyby. Therefore, their measurements could be deemed as one observation point during the Earth flyby.** The two spacecraft will be separated when they are scheduled to insert into Mercury's orbit by late 2025 or early 2026.

This study uses measurements collected by the magnetometer (MAG) onboard MPO (Heyner et al., 2021), and the low energy electron by Mercury Electron Analyzer (MEA) (Sauvaud et al., 2010), which is part of the Mercury Plasma Particle Experiment (MPPE) onboard Mio (Saito et al., 2021). The MPO/MAG includes one outboard sensor and one inboard sensor, and it has a sampling rate of 128 Hz. Mio/MEA has a sampling rate of 4 s. The IMF and solar wind conditions are obtained from the OMNI dataset (King and Papitashvili, 2005), which has a time resolution of 1 minute.

2.2. Overview of Magnetosheath and Magnetopause

Figure 1 shows an overview of the dayside magnetopause crossing during BepiColombo's Earth flyby. BepiColombo traveled from the magnetosheath into the dayside magnetosphere. It crossed the magnetopause at a distance of ~ 4.8 R_E dawnward from the subsolar magnetopause, which corresponded to a position of (11.2, -4.8, -0.3) R_E in the GSM coordinate. During the 30 minutes interval around the magnetopause crossing (~00:05 to 00:35 UT) analyzed here, the IMF was southward with a strong radial component. The B_x was the dominant component ($B_x/B_t > 0.7$ in Figure 1h). The average electron density in the magnetosheath was estimated to be ~ 10 cm^{-3} based on the onboard-calculated partial moment from Mio/MEA between 00:05 and 00:28. The magnetosheath plasma β was high with a value of ~ 8.0, which was the ratio of the thermal pressure to the magnetic pressure. The thermal pressure in the magnetosheath was calculated by assuming that the pressure balance existed across the dayside magnetopause and that the thermal pressure inside the dayside magnetosphere was negligible compared to the magnetic pressure.

3. Magnetopause Reconnections and FTE-type Flux Ropes

3.1. Identification of FTE-type Flux Ropes

The FTE-type flux ropes were identified after the measured magnetic field was rotated into boundary normal coordinates (the LMN coordinate). The minimum variance analysis (MVA) (Sonnerup and Cahill Jr., 1967; Sonnerup and Scheible, 1998) was performed on the magnetic field measurements across the magnetopause current sheet from 00:32:30 to 00:33:25 UT to obtain the LMN coordinate. The MVA results produced L =

[0.10, 0.24, 0.97] (maximum variance direction), M = [0.12, 0.96, -0.25] (intermediate variance direction), N = [0.99, -0.14, -0.06] (minimum variance direction), and the eigenvalue ratios were $\lambda_{max}/\lambda_{int}$ ~ 54.3, $\lambda_{int}/\lambda_{min}$ ~ 3.9. Both of the ratios were larger than 3 indicating that the LMN coordinate of the magnetopause was well determined [*Sonnerup & Scheible*, 1998].

The FTE-type flux ropes were identified with bipolar signatures in the normal magnetic field (B_N) and clear magnetic field rotation (Russell and Elphic, 1978). The identification of flux ropes also required the signature of a strong magnetic field along their central axis, i.e. the intermediate variance direction [**see Figure 2 for an example**, e.g. *Akhavan-Tafti et al.*, 2018]. Six FTE-type flux ropes were identified in this manner in the magnetosheath just upstream of the dayside magnetopause and marked with green arrows in Figure 1e and listed in Table 1.

The first FTE-type flux rope shown in Figure 2 was centered at ~ 00:11:04 UT when the IMF clock angle was ~ 210°, and B_x/B_t ~ 0.75. **This flux rope traveled southward as inferred from the polarities of the B_N variation (negative to positive, Figure 2c). The flux rope corresponded to clear enhancement in B_M (Figure 2b) and field rotation in the plane of B_{max}-B_{int} (Figure 2e).** About 2 minutes later, the clock angle increased to ~ 260°. This IMF orientation persisted for about 12 minutes, during which no FTE-type flux ropes were observed. At ~ 00:26:06 UT, the clock angle decreased from ~ 260° to ~ 210° while the ratio of B_x/B_t increased to ~ 0.90. At this point, 5 FTE-type flux ropes successively appeared up to the point where the magnetopause was crossed. The direction of travel for these 5 flux ropes was inferred to be northward, again based on the B_N variations. The first flux rope traveled southward indicating that the primary magnetopause X-line was initially located northward of the spacecraft. Later, the northward motion of the 5 flux ropes indicated that the primary magnetopause X-line(s) had shifted southward.

3.2. Reconnection X-lines from Maximum Magnetic Shear Model

To further investigate reconnection during BepiColombo's dayside magnetopause traversal, the maximum magnetic shear model (Trattner et al., 2007; 2017) was employed to deduce the location of the reconnection X-lines. The magnetic shear angle plots during the intervals centered at 00:09, 00:20, 00:28 UT are shown in Figure 3. Figures 3a and 3b corresponded to a distorted feature of the anti-parallel reconnection region, which has recently been termed a "Knee" event (Trattner et al., 2021). The bent shape of the anti-parallel reconnection region is associated with the field line draping in the magnetosheath during the dominant B_x (significantly sunward) component in this period. **In Figure 3c, we did not provide the predicted X-line. This was because a continuous X-line along the maximum magnetic shear location was difficult to obtain under the situation of a B_x/B_t > 0.9, which was due to the lack of comprehensive study on how the significant radial IMF draping around the magnetopause influences magnetic reconnection.**

In Figure 3a, BepiColombo was located southward of the predicted X-line. From Figure 3a to Figure 3b, the predicted X-line crossed the location of BepiColombo and was then located to the south of BepiColombo. The changes in X-line locations from Figures 3a to 3b are due to the IMF clock angle decreasing around 10° together with the B_x/B_t increasing from 0.78 to 0.86.

The direction of motion for our FTE-type flux ropes was consistent with the predicted location of the reconnection X-line predicted by the maximum magnetic shear model during the changing solar wind conditions for this

magnetopause encounter. Figure 3a corresponded to the only southward traveling FTE-type flux rope, while the other five northward traveling FTE-type flux ropes were observed during the conditions shown in Figures 3b and 3c. **It needs to note that the FTE-type flux ropes and reconnection exhausts should correspond to strong lateral motion as the predicted X-lines were significantly along with the north-south direction. The reconnection exhausts would correspond to a strong duskward component when the spacecraft was located southward of the X-line and a strong dawnward component when it was northward of the X-line.** Although the maximum magnetic shear model faces challenges in determining the draping magnetic field lines in the magnetosheath during the intervals of the dominant B_x component (Trattner et al., 2007; 2012), the model predictions are consistent with our observations during BepiColombo's crossing.

3.3. FTE-type Flux Rope Modeling

This study employed a force-free flux rope model (Kivelson and Khurana, 1995) to fit the FTE-type flux ropes. This flux rope model starts from the periodic pinch solution (Schindler et al., 1973) of Ampere's law ($\nabla \times \vec{B} = \mu_0 \vec{J}$), where $\vec{B}$ is the magnetic field vector, $\vec{J}$ is the current density vector, and μ_0 is the magnetic permeability in the vacuum. Kivelson and Khurana (1995) further include the axial magnetic field component (B_{int}) in the periodic pinch solution. The flux rope model introduced by Kivelson and Khurana (1995) does not consider the gradient of the magnetic field along the axis of the flux rope. The self-consistent solution of the flux rope model is

$$\begin{cases} B_{max} = \left(\frac{B_T}{\chi}\right)\sqrt{1+\epsilon^2}\,\sinh\left(\frac{x_{min}}{T}\right) \\ B_{int} = \left(\frac{B_T}{\chi}\right)\sqrt{1+\left(\frac{B_{int0}\chi}{B_T}\right)^2} \\ B_{min} = \left(\frac{B_T}{\chi}\right)\epsilon\,\sin\left(\frac{x_{max}}{T}\right) \end{cases} \quad (1)$$

In the equation, the x_{min} and x_{max} are the positions in the flux rope along with $\vec{n}_{min}$ and $\vec{n}_{max}$. The $\vec{n}_{min}$, $\vec{n}_{int}$ and $\vec{n}_{max}$ refer to the local coordinate of the flux rope. The T is the vertical scale of the flux rope along with the $\vec{n}_{max}$ and the B_T is the magnetic field intensity near the boundary of the flux rope along with the $\vec{n}_{min}$. The B_{int0} is the B_{int} in the background. The χ is

$$\chi = \epsilon\cos\left(\frac{x_{max}}{T}\right) + \sqrt{1+\epsilon^2}\,\cosh\left(\frac{x_{min}}{T}\right) \quad (2)$$

In this equation, the parameter ε is associated with the shape of the flux rope, i.e., from flattened to circular profiles. The axial flux content (Φ_{axial}) is calculated by integrating the axial field (B_{int}) over the entire flux rope area,

$$\Phi_{axial} = \int B_{int}\,dS \quad (3)$$

During the fitting, we assume that the traveling speed of flux ropes was 100 km/s, which corresponds to the average Alfvén speed in the sub-solar magnetosheath. **The traveling speed is required in calculating the scales and magnetic flux content for the flux ropes.** The least-squares of the minimization of the magnetic field differences (X^2) is employed to define the best fit, which is calculated from

$$X^2 = \frac{\sum_{i=1}^{N_{point}} \sum_{j}^{max,int,min} \left[\left(B_j(i) - B'_j(i) \right) / B_t(i) \right]^2}{N_{point}} \quad (4)$$

where B_{max}, B_{int}, B_{min}, and B_t are the components and magnitude of the measured magnetic fields and B'_{max}, B'_{int}, and B'_{min} are the components of the magnetic fields from the model. The N_{point} is the number of data points. We set up a threshold of $X^2 < 0.1$ to be the successful modeling.

Different from the circular profile of flux ropes resulting from the Lundquist force-free flux rope model (Lundquist, 1950; Burlaga, 1988; Lepping et al., 1990), this force-free model can give either flattened or circular profiles of the flux rope. We use the semi-minor and semi-major to refer to the flattened features. **The semi-major corresponds to the scale of flux rope along with $\vec{n}_{min}$, which is close to L direction of the magnetopause. The semi-minor correspond to the scale of flux rope along with $\vec{n}_{max}$, which is close to the N direction of the magnetopause.** This flux rope model is successfully applied for the flux ropes in Earth's plasma sheet (Kivelson and Khurana, 1995), on Earth's magnetopause (Zhang et al., 2008), and in Mercury's plasma sheet (Zhao et al., 2019).

Out of the 6 FTE-type flux ropes, 4 were successfully modeled. **As an example, the modeling curves of the flux rope centered at 00:28:13 UT are shown in Figures 4a to 4d. In the figures, the dashed lines overlapping with the solid measured magnetic fields represent the modeling curves from the flux rope model. It can be seen clearly that the two curves were close to each other and this flux rope was well fitted by the model.** The modeling results for the 4 flux ropes were summarized in Table 1. The plasma density was ~ 10 cm^{-3} corresponding to an ion inertial length (d_i) of ~ 70 km. The two FTE-type flux ropes centered at 00:26:06 UT and 00:26:26 UT were in the scales of several d_i. The magnetic flux content of these two flux ropes was small (~ 20 kWb). In addition, these two flux ropes corresponded to the largest and smallest core fields. The other two FTE-type flux ropes centered at 00:28:13 UT and 00:30:26 UT were in the scales of more than 10 d_i. These two flux ropes contained much higher magnetic flux (~ 300 kWb and ~ 188 kWb). The analysis of the flux rope centered at ~ 00:28:13 UT corresponding to the highest magnetic flux content is shown in the next section. Moreover, the flux ropes centered at 00:26:06 UT, 00:26:26 UT, and 00:30:26 UT, are close to circular profiles with the semi-minor slightly smaller than the semi-major. The flux rope centered at ~ 00:28:13 UT includes the strongest flatten profile.

3.4. Coalescence Event

Figure 4 shows the magnetic field measurements of the FTE-type flux rope centered at ~ 00:28:13 UT in the LMN coordinate, which corresponds to the fifth green arrow counting from the leftside in Figure 1e. Figure 4c showed that the B_N included two successive bipolar signatures, which implied that two smaller scale flux ropes were merging. Indeed, the hodogram in the B_{max}-B_{int} plane in Figure 4f confirmed the field rotations of two flux ropes, named "FR#A" and "FR#B". Figure 4e further illustrated the merging of the two flux ropes and the trajectory of BepiColombo. The magenta arrows and shaded region in Figure 4e indicated the secondary reconnection between FR#A and FR#B. This FTE-type flux rope with the highest flux content possibly resulted from the coalescence of two smaller-scale flux ropes.

In order to study how well aligned FR#A and FR#B were, we applied the MVA on FR#A and FR#B separately. The eigenvalue ratios were $\lambda_{max}/\lambda_{int}$ ~ 1.91 and $\lambda_{int}/\lambda_{min}$ ~ 21.7 for FR#A from 00:28:03 to

00:28:09. The eigenvalue ratios were $\lambda_{max}/\lambda_{int}$ ~ 3.34 and $\lambda_{int}/\lambda_{min}$ ~ 12.6 for FR#B from 00:28:09 to 00:28:16. The large values of $\lambda_{int}/\lambda_{min}$ indicated that the $\vec{n}_{min}$ were well determined for both flux ropes, in which $\vec{n}_{min}$ = [-0.20,-0.58,-0.79] for FR#A and $\vec{n}_{min}$= [0.23,-0.55,-0.80] for FR#B. The $\vec{n}_{min}$ were close to each other with a separation angle of 25°. The $\vec{n}_{min}$ obtained for the coalescence event was [-0.04,-0.49,-0.87], which were 12° and 17° away from the $\vec{n}_{min}$ of FR#A and FR#B separately. The small separations of the $\vec{n}_{min}$ should indicate that FR#A and FR#B were well aligned. It needs to note that the coalescence signature was only observed in this FTE-type flux rope centered at ~ 00:28:13 UT. We did not see similar successive bipolar signatures of the B_N in other 5 FTE-type flux ropes.

3.5. Magnetopause Reconnection and Secondary Magnetic Reconnection

In Figure 5, the properties of the secondary current sheet in the coalescence event (Figure 4) and the magnetopause current sheet are studied. For the secondary current sheet, the eigenvalue ratios of $\lambda_{max}/\lambda_{int}$ ~ 6.4, $\lambda_{int}/\lambda_{min}$ ~ 11.0 resulting from the MVA were both larger than 3 indicating the local coordinate of the secondary current sheet was well built. The magnetic field measurements of the magnetopause current sheet were shown in the LMN coordinate. In the reconnecting current sheet, the dimensionless reconnection rate can be determined from the ratio of the normal magnetic field component (B_{normal}) to the reconnecting magnetic field (B_{inflow}) in the inflow region (Sonnerup, 1974; Sonnerup et al., 1981; Fuselier and Lewis, 2011; Phan et al., 2001). In the secondary current sheet (Figures 5a to 5d), the B_{normal} was ~ 5 nT (the B_{min} averaged from 00:28:08.8 to 00:28:09.6 UT). Here the average B_t from 00:28:09.8 to 00:28:10.4 UT was taken as the B_{inflow} (~ 36 nT). The dimensionless reconnection rate was ~ 0.14 if the reconnection occurred in the secondary current sheet. Meanwhile, the intensity of the guide field (B_{int}, Figure 5b) was ~ 32 nT across the current sheet, which was ~ 0.89 when normalized to the B_{inflow}. In the magnetopause current sheet, the B_{normal} was 8.3 nT (averaged B_N from 00:32:56 to 00:33:05 UT, Figure 5g). The B_{inflow} in the magnetosphere side adjacent to the magnetopause was ~ 46.1 nT (average B_t from 00:33:06 to 00:33:15 UT, Figure 5h). Thus, the dimensionless reconnection rate was calculated to be ~ 0.18. The guide field across the magnetopause was ~ 13 nT, which was 0.28 normalized to the B_{inflow}.

However, it needed to point out that the estimation of reconnection rate based on B_N/B_{inflow} could be imprecise. For example, the uncertainties of the normal direction and the fluctuations in the field strength could influence the accuracy of the reconnection rates. As noted by Sonnerup and Scheible (1998) and Khrabrov and Sonnerup (1998), there were uncertainties in the eigenvectors determined by the MVA, which could be either statistical error or the magnetic structure was not perfectly stationary and one-dimensional. By employing the method introduced by Khrabrov and Sonnerup (1998), we obtained an uncertainty of ~ 0.93 nT for the B_{normal} of the secondary current sheet and ~ 0.04 nT for the magnetopause current sheet. However, it was not certain that magnetic reconnection was occurring in the secondary current sheet or the magnetopause current sheet. There was no complimentary evidence for the magnetic reconnection since the measurements from BepiColombo were limited during the Earth flyby. The low energy electron measurements (Mio/MEA) were limited in the field of view and the time resolution was ~ 4 seconds. The MEA could not provide a complete distribution relative to the background magnetic field and its time

resolution was much longer than the time scale of the secondary current sheet. Therefore, the conclusions obtained about magnetic reconnection were tentative and further analysis about a similar event was needed, especially those measurements taken from the MMS.

4. Conclusions and Discussions

Our analysis of the subsolar magnetopause observations during BepiColombo's Earth flyby has produced several conclusions.

First, the BepiColombo's dayside magnetopause crossing took place during an interval with high plasma β (~ 8) conditions in the magnetosheath and a strong radial IMF component ($B_x/B_{tot} > 0.75$). The traveling of the FTE-type flux rope suggests that the X-line crosses the location of BepiColombo, which is in close agreement with the predictions of the maximum magnetic shear model. The motion of the X-line is associated with the rotation and the increase in the B_x of the IMF. BepiColombo crosses the magnetopause near the magnetic equator, and 10 April 2020 is close to the spring equinox, which indicates a small dipole tilt influence. These observations of the crossing of the X-line provide clear evidence of magnetic reconnection near the magnetic equator under a strong radial IMF.

Second, the properties of the FTE-type flux ropes are fit using a force-free flux rope model introduced by Kivelson and Khurana (1995). The FTE-type flux ropes correspond to scales ranging from several d_i to around 20 d_i, and the FTE-type flux rope with a large scale and the highest magnetic flux content exhibited very clear coalescence signatures. These observations strongly support the theories in which the FTE-type flux ropes grow in scales and magnetic flux contents through coalescence.

Third, the secondary reconnection producing the coalescence event and the magnetopause current sheet are investigated. The reconnection rate of the secondary reconnection (0.14) is comparable with the reconnection rate of dayside magnetopause (0.18). However, the secondary reconnection corresponds to a larger normalized guide field (0.89) and a magnetopause reconnection (0.28). **There is no complimentary evidence that magnetic reconnection is occurring in the secondary current sheet and magnetopause current sheet; therefore, the conclusions about magnetic reconnection are tentative.**

The large guide fields observed by BepiColombo are likely a common feature of the secondary magnetic reconnection during the coalescence. For example, Zhou et al. (2017) reported a coalescence event with a strong guide field. We suggest that these large guide fields should be included in future simulations, which investigate the particle energizations due to e coalescence. The large guide fields may influence the reconnection rate as suggested by Pritchett and Coroniti (2004) and Ricci et al. (2004), and therefore affect the energization of particles during the coalescence. Furthermore, a recent investigation also suggests that a large guide field might limit the ability of Fermi acceleration during the coalescence (Montag et al., 2017).

The FTE-type flux rope containing the coalescence signature has a scale of ~20 d_i. Therefore, the secondary reconnecting current sheet embedded within the FTE-type flux rope is likely with a scale much smaller than 20 d_i. We want to note that the secondary reconnection during the coalescence of flux ropes share some similarities with the electron-only reconnection associated with the magnetosheath turbulence, whose reconnecting current sheet has scales (< 10 d_i) and a large guide field as revealed by MMS measurements (Phan et al., 2018; Stawarz et al., 2019)

and simulations (Califano et al., 2020). Therefore, it is likely that the secondary reconnection associated with coalescence is also electron-only magnetic reconnection, which certainly deserves a detailed study.

Data availability

The measurements from Mio/MEA and MPO/MAG analyzed in this study are available in the supporting information. The data archiving is underway. Mio/MEA data will be able to be accessed from the AMDA science analysis system (http://amda.cdpp.eu) provided by the Centre de Données de la Physique des Plasmas (CDPP) supported by CNRS, CNES, Observatoire de Paris, and Université Paul Sabatier Toulouse. MPO/MAG data will be available from https://archives.esac.esa.int/psa/#!Home%20View. OMNI dataset is available at https://omniweb.gsfc.nasa.gov/.

Author contributions

W. J. S. led the work, identified the events, conducted the data analysis of the dataset, and wrote the manuscript. W. J. S., J. A. S., and R. N. jointly designed the work. D. H. and J. Z. D. M. provided knowledge of the MPO-MAG instrument and the MPO-MAG data. S. A. and N. A. provided knowledge of the Mio-MEA instrument and the Mio-MEA data. K. J. T. provided Figure 3 and the relevant descriptions. J. T. Z. performed force-free fittings of the flux ropes. All authors discussed and contributed to the manuscript.

Competing interests

The authors declare no competing interests.

Acknowledgment

The BepiColombo project is supported by ESA and JAXA. W. J. S. and J. A. S. were supported by NASA Grants NNX16AJ67G and 80NSSC18K1137. N.A. and S.A. acknowledge the support of CNES for the BepiColombo mission. The research at LASP (K. J. T.) is supported by NASA grants NNG04EB99C and 80NSSC20K0688. W. J. S. thanks Dr. Gangkai Poh for helpful discussions.

References.

Akhavan-Tafti, M., Slavin, J. A., Le, G., Eastwood, J. P., Strangeway, R. J., Russell, C. T., Nakamura, R., Baumjohann, W., Torbert, R. B., Giles, B. L., Gershman, D. J., and Burch, J. L.: MMS Examination of FTEs at the Earth's Subsolar Magnetopause, J Geophys Res Space Phys, 123, 1224-1241, 10.1002/2017JA024681, 2018.

Belenkaya, E. S.: Reconnection modes for near-radial interplanetary magnetic field, J Geophys Res Space Phys, 103, 26487-26494, https://doi.org/10.1029/98JA02270, 1998.

Benkhoff, J., van Casteren, J., Hayakawa, H., Fujimoto, M., Laakso, H., Novara, M., Ferri, P., Middleton, H. R., and Ziethe, R.: BepiColombo—Comprehensive exploration of Mercury: Mission overview and science goals, Planet Space Sci, 58, 2-20, https://doi.org/10.1016/j.pss.2009.09.020, 2010.
Biskamp, D. and Welter, H.: Coalescence of Magnetic Islands, Phys Rev Lett, 44, 1069-1072, 10.1103/PhysRevLett.44.1069, 1980.
Burch, J. L., Moore, T. E., Torbert, R. B., and Giles, B. L.: Magnetospheric Multiscale Overview and Science Objectives, Space Sci Rev, 199, 5-21, 10.1007/s11214-015-0164-9, 2016.
Burlaga, L. F.: Magnetic clouds and force-free fields with constant alpha, J Geophys Res Space Phys, 93, 7217-7224, 10.1029/JA093iA07p07217, 1988.
Califano, F., Cerri, S. S., Faganello, M., Laveder, D., Sisti, M., and Kunz, M. W.: Electron-Only Reconnection in Plasma Turbulence, Front Phys, 8, 10.3389/fphy.2020.00317, 2020.
Dorelli, J. C. and Bhattacharjee, A.: On the generation and topology of flux transfer events, J Geophys Res Space Phys, 114, https://doi.org/10.1029/2008JA013410, 2009.
Drake, J. F., Swisdak, M., Che, H., and Shay, M. A.: Electron acceleration from contracting magnetic islands during reconnection, Nature, 443, 553, 10.1038/nature05116, 2006.
Dungey, J. W.: Interplanetary Magnetic Field and the Auroral Zones, Phys Rev Lett, 6, 47-48, 10.1103/PhysRevLett.6.47, 1961.
Fear, R. C., Trenchi, L., Coxon, J. C., and Milan, S. E.: How Much Flux Does a Flux Transfer Event Transfer?, J Geophys Res Space Phys, 122, 12,310-312,327, doi:10.1002/2017JA024730, 2017.
Fermo, R. L., Drake, J. F., Swisdak, M., and Hwang, K. J.: Comparison of a statistical model for magnetic islands in large current layers with Hall MHD simulations and Cluster FTE observations, J Geophys Res Space Phys, 116, 10.1029/2010JA016271, 2011.
Fuselier, S. A. and Lewis, W. S.: Properties of Near-Earth Magnetic Reconnection from In-Situ Observations, Space Sci Rev, 160, 95, 10.1007/s11214-011-9820-x, 2011.
Gou, X. C., Shi, Q. Q., Tian, A. M., Sun, W. J., Dunlop, M. W., Fu, S. Y., Zong, Q. G., Facskó, G., Nowada, M., Pu, Z. Y., Mailyan, B., Xiao, T., and Shen, X. C.: Solar wind plasma entry observed by cluster in the high-latitude magnetospheric lobes, J Geophys Res Space Phys, 121, 4135-4144, https://doi.org/10.1002/2015JA021578, 2016.
Heyner, D., Auster, H. U., Fornaçon, K. H., Carr, C., Richter, I., Mieth, J. Z. D., Kolhey, P., Exner, W., Motschmann, U., Baumjohann, W., Matsuoka, A., Magnes, W., Berghofer, G., Fischer, D., Plaschke, F., Nakamura, R., Narita, Y., Delva, M., Volwerk, M., Balogh, A., Dougherty, M., Horbury, T., Langlais, B., Mandea, M., Masters, A., Oliveira, J. S., Sánchez-Cano, B., Slavin, J. A., Vennerstrøm, S., Vogt, J., Wicht, J., and Glassmeier, K. H.: The BepiColombo Planetary Magnetometer MPO-MAG: What Can We Learn from the Hermean Magnetic Field?, Space Sci Rev, 217, 52, 10.1007/s11214-021-00822-x, 2021.
Hoilijoki, S., Ganse, U., Pfau-Kempf, Y., Cassak, P. A., Walsh, B. M., Hietala, H., von Alfthan, S., and Palmroth, M.: Reconnection rates and X line motion at the magnetopause: Global 2D-3V hybrid-Vlasov simulation results, J Geophys Res Space Phys, 122, 2877-2888, https://doi.org/10.1002/2016JA023709, 2017.
Imber, S. M., Slavin, J. A., Boardsen, S. A., Anderson, B. J., Korth, H., McNutt Jr., R. L., and Solomon, S. C.: MESSENGER observations of large dayside flux transfer events: Do they drive Mercury's substorm cycle?, J Geophys Res Space Phys, 119, 5613-5623, 10.1002/2014ja019884, 2014.
Jasinski, J. M., Akhavan-Tafti, M., Sun, W., Slavin, J. A., Coates, A. J., Fuselier, S. A., Sergis, N., and Murphy, N.: Flux Transfer Events at a Reconnection-Suppressed Magnetopause: Cassini Observations at Saturn, J Geophys Res Space Phys, 126, e2020JA028786, https://doi.org/10.1029/2020JA028786, 2021.
Jasinski, J. M., Slavin, J. A., Arridge, C. S., Poh, G., Jia, X., Sergis, N., Coates, A. J., Jones, G. H., and Waite Jr., J. H.: Flux transfer event observation at Saturn's dayside magnetopause by the Cassini spacecraft, Geophys Res Lett, 43, 6713-6723, doi:10.1002/2016GL069260, 2016.
Kacem, I., Jacquey, C., Génot, V., Lavraud, B., Vernisse, Y., Marchaudon, A., Le Contel, O., Breuillard, H., Phan, T. D., Hasegawa, H., Oka, M., Trattner, K. J., Farrugia, C. J., Paulson, K., Eastwood, J. P., Fuselier, S. A., Turner, D., Eriksson, S., Wilder, F., Russell, C. T., Øieroset, M., Burch, J., Graham, D. B., Sauvaud, J. A., Avanov, L., Chandler, M., Coffey, V., Dorelli, J., Gershman, D. J., Giles, B. L., Moore, T.

E., Saito, Y., Chen, L. J., and Penou, E.: Magnetic Reconnection at a Thin Current Sheet Separating Two Interlaced Flux Tubes at the Earth's Magnetopause, J Geophys Res Space Phys, 123, 1779-1793, 10.1002/2017JA024537, 2018.
Khrabrov, A. V. and Sonnerup, B. U. Ö.: Error estimates for minimum variance analysis, J Geophys Res Space Phys, 103, 6641-6651, https://doi.org/10.1029/97JA03731, 1998.
King, J. H. and Papitashvili, N. E.: Solar wind spatial scales in and comparisons of hourly Wind and ACE plasma and magnetic field data, J Geophys Res Space Phys, 110, 10.1029/2004ja010649, 2005.
Kivelson, M. G. and Khurana, K. K.: Models of flux ropes embedded in a harris neutral sheet: Force-free solutions in low and high beta plasmas, J Geophys Res Space Phys, 100, 23637-23645, https://doi.org/10.1029/95JA01548, 1995.
Kuo, H., Russell, C. T., and Le, G.: Statistical studies of flux transfer events, J Geophys Res Space Phys, 100, 3513-3519, https://doi.org/10.1029/94JA02498, 1995.
Lai, H. R., Wei, H. Y., Russell, C. T., Arridge, C. S., and Dougherty, M. K.: Reconnection at the magnetopause of Saturn: Perspective from FTE occurrence and magnetosphere size, J Geophys Res Space Phys, 117, 10.1029/2011ja017263, 2012.
Lee, L. C. and Fu, Z. F.: A theory of magnetic flux transfer at the Earth's magnetopause, Geophys Res Lett, 12, 105-108, 10.1029/GL012i002p00105, 1985.
Lee, L. C., Ma, Z. W., Fu, Z. F., and Otto, A.: Topology of magnetic flux ropes and formation of fossil flux transfer events and boundary layer plasmas, J Geophys Res Space Phys, 98, 3943-3951, https://doi.org/10.1029/92JA02203, 1993.
Lepping, R. P., Jones, J. A., and Burlaga, L. F.: Magnetic field structure of interplanetary magnetic clouds at 1 AU, J Geophys Res Space Phys, 95, 11957-11965, 10.1029/JA095iA08p11957, 1990.
Lockwood, M., Cowley, S. W. H., Smith, M. F., Rijnbeek, R. P., and Elphic, R. C.: The contribution of flux transfer events to convection, Geophys Res Lett, 22, 1185-1188, 10.1029/95gl01008, 1995.
Luhmann, J. G., Walker, R. J., Russell, C. T., Crooker, N. U., Spreiter, J. R., and Stahara, S. S.: Patterns of potential magnetic field merging sites on the dayside magnetopause, J Geophys Res Space Phys, 89, 1739-1742, https://doi.org/10.1029/JA089iA03p01739, 1984.
Lundquist, S.: Magnetohydrostatic fields, Ark. Fys., 2, 361-365, 1950.
Mangano, V., Dósa, M., Fränz, M., Milillo, A., Oliveira, J. S., Lee, Y. J., McKenna-Lawlor, S., Grassi, D., Heyner, D., Kozyrev, A. S., Peron, R., Helbert, J., Besse, S., de la Fuente, S., Montagnon, E., Zender, J., Volwerk, M., Chaufray, J.-Y., Slavin, J. A., Krüger, H., Maturilli, A., Cornet, T., Iwai, K., Miyoshi, Y., Lucente, M., Massetti, S., Schmidt, C. A., Dong, C., Quarati, F., Hirai, T., Varsani, A., Belyaev, D., Zhong, J., Kilpua, E. K. J., Jackson, B. V., Odstrcil, D., Plaschke, F., Vainio, R., Jarvinen, R., Ivanovski, S. L., Madár, Á., Erdős, G., Plainaki, C., Alberti, T., Aizawa, S., Benkhoff, J., Murakami, G., Quemerais, E., Hiesinger, H., Mitrofanov, I. G., Iess, L., Santoli, F., Orsini, S., Lichtenegger, H., Laky, G., Barabash, S., Moissl, R., Huovelin, J., Kasaba, Y., Saito, Y., Kobayashi, M., and Baumjohann, W.: BepiColombo Science Investigations During Cruise and Flybys at the Earth, Venus and Mercury, Space Sci Rev, 217, 23, 10.1007/s11214-021-00797-9, 2021.
Milillo, A., Fujimoto, M., Murakami, G., Benkhoff, J., Zender, J., Aizawa, S., Dósa, M., Griton, L., Heyner, D., Ho, G., Imber, S. M., Jia, X., Karlsson, T., Killen, R. M., Laurenza, M., Lindsay, S. T., McKenna-Lawlor, S., Mura, A., Raines, J. M., Rothery, D. A., André, N., Baumjohann, W., Berezhnoy, A., Bourdin, P. A., Bunce, E. J., Califano, F., Deca, J., de la Fuente, S., Dong, C., Grava, C., Fatemi, S., Henri, P., Ivanovski, S. L., Jackson, B. V., James, M., Kallio, E., Kasaba, Y., Kilpua, E., Kobayashi, M., Langlais, B., Leblanc, F., Lhotka, C., Mangano, V., Martindale, A., Massetti, S., Masters, A., Morooka, M., Narita, Y., Oliveira, J. S., Odstrcil, D., Orsini, S., Pelizzo, M. G., Plainaki, C., Plaschke, F., Sahraoui, F., Seki, K., Slavin, J. A., Vainio, R., Wurz, P., Barabash, S., Carr, C. M., Delcourt, D., Glassmeier, K. H., Grande, M., Hirahara, M., Huovelin, J., Korablev, O., Kojima, H., Lichtenegger, H., Livi, S., Matsuoka, A., Moissl, R., Moncuquet, M., Muinonen, K., Quèmerais, E., Saito, Y., Yagitani, S., Yoshikawa, I., and Wahlund, J. E.: Investigating Mercury's Environment with the Two-Spacecraft BepiColombo Mission, Space Sci Rev, 216, 93, 10.1007/s11214-020-00712-8, 2020.

Montag, P., Egedal, J., Lichko, E., and Wetherton, B.: Impact of compressibility and a guide field on Fermi acceleration during magnetic island coalescence, Phys Plasmas, 24, 062906, 10.1063/1.4985302, 2017.
Murakami, G., Hayakawa, H., Ogawa, H., Matsuda, S., Seki, T., Kasaba, Y., Saito, Y., Yoshikawa, I., Kobayashi, M., Baumjohann, W., Matsuoka, A., Kojima, H., Yagitani, S., Moncuquet, M., Wahlund, J.-E., Delcourt, D., Hirahara, M., Barabash, S., Korablev, O., and Fujimoto, M.: Mio—First Comprehensive Exploration of Mercury's Space Environment: Mission Overview, Space Sci Rev, 216, 113, 10.1007/s11214-020-00733-3, 2020.
Øieroset, M., Phan, T. D., Haggerty, C., Shay, M. A., Eastwood, J. P., Gershman, D. J., Drake, J. F., Fujimoto, M., Ergun, R. E., Mozer, F. S., Oka, M., Torbert, R. B., Burch, J. L., Wang, S., Chen, L. J., Swisdak, M., Pollock, C., Dorelli, J. C., Fuselier, S. A., Lavraud, B., Giles, B. L., Moore, T. E., Saito, Y., Avanov, L. A., Paterson, W., Strangeway, R. J., Russell, C. T., Khotyaintsev, Y., Lindqvist, P. A., and Malakit, K.: MMS observations of large guide field symmetric reconnection between colliding reconnection jets at the center of a magnetic flux rope at the magnetopause, Geophys Res Lett, 43, 5536-5544, https://doi.org/10.1002/2016GL069166, 2016.
Paschmann, G., Haerendel, G., Papamastorakis, I., Sckopke, N., Bame, S. J., Gosling, J. T., and Russell, C. T.: Plasma and magnetic field characteristics of magnetic flux transfer events, J Geophys Res Space Phys, 87, 2159-2168, https://doi.org/10.1029/JA087iA04p02159, 1982.
Phan, T. D., Sonnerup, B. U. Ö., and Lin, R. P.: Fluid and kinetics signatures of reconnection at the dawn tail magnetopause: Wind observations, J Geophys Res Space Phys, 106, 25489-25501, https://doi.org/10.1029/2001JA900054, 2001.
Phan, T. D., Eastwood, J. P., Shay, M. A., Drake, J. F., Sonnerup, B. U. Ö., Fujimoto, M., Cassak, P. A., Øieroset, M., Burch, J. L., Torbert, R. B., Rager, A. C., Dorelli, J. C., Gershman, D. J., Pollock, C., Pyakurel, P. S., Haggerty, C. C., Khotyaintsev, Y., Lavraud, B., Saito, Y., Oka, M., Ergun, R. E., Retino, A., Le Contel, O., Argall, M. R., Giles, B. L., Moore, T. E., Wilder, F. D., Strangeway, R. J., Russell, C. T., Lindqvist, P. A., and Magnes, W.: Electron magnetic reconnection without ion coupling in Earth's turbulent magnetosheath, Nature, 557, 202-206, 10.1038/s41586-018-0091-5, 2018.
Pi, G., Shue, J.-H., Grygorov, K., Li, H.-M., Němeček, Z., Šafránková, J., Yang, Y.-H., and Wang, K.: Evolution of the magnetic field structure outside the magnetopause under radial IMF conditions, J Geophys Res Space Phys, 122, 4051-4063, https://doi.org/10.1002/2015JA021809, 2017.
Poh, G., Slavin, J. A., Lu, S., Le, G., Ozturk, D. S., Sun, W.-J., Zou, S., Eastwood, J. P., Nakamura, R., Baumjohann, W., Russell, C. T., Gershman, D. J., Giles, B. L., Pollock, C. J., Moore, T. E., Torbert, R. B., and Burch, J. L.: Dissipation of Earthward Propagating Flux Rope Through Re-reconnection with Geomagnetic Field: An MMS Case Study, J Geophys Res Space Phys, 124, 7477-7493, https://doi.org/10.1029/2018JA026451, 2019.
Pritchett, P. L. and Coroniti, F. V.: Three-dimensional collisionless magnetic reconnection in the presence of a guide field, J Geophys Res Space Phys, 109, 10.1029/2003ja009999, 2004.
Raeder, J.: Flux Transfer Events: 1. generation mechanism for strong southward IMF, Ann. Geophys., 24, 381-392, 10.5194/angeo-24-381-2006, 2006.
Ricci, P., Brackbill, J. U., Daughton, W., and Lapenta, G.: Collisionless magnetic reconnection in the presence of a guide field, Phys Plasmas, 11, 4102-4114, 10.1063/1.1768552, 2004.
Rijnbeek, R. P., Cowley, S. W. H., Southwood, D. J., and Russell, C. T.: A survey of dayside flux transfer events observed by ISEE 1 and 2 magnetometers, J Geophys Res Space Phys, 89, 786-800, 10.1029/JA089iA02p00786, 1984.
Russell, C. T. and Elphic, R. C.: Initial ISEE magnetometer results: magnetopause observations, Space Sci Rev, 22, 681-715, 10.1007/BF00212619, 1978.
Russell, C. T. and Walker, R. J.: Flux transfer events at Mercury, J Geophys Res Space Phys, 90, 11067-11074, 10.1029/JA090iA11p11067, 1985.
Saito, Y., Delcourt, D., Hirahara, M., Barabash, S., André, N., Takashima, T., Asamura, K., Yokota, S., Wieser, M., Nishino, M. N., Oka, M., Futaana, Y., Harada, Y., Sauvaud, J.-A., Louarn, P., Lavraud, B., Génot, V., Mazelle, C., Dandouras, I., Jacquey, C., Aoustin, C., Barthe, A., Cadu, A., Fedorov, A.,

Frezoul, A.-M., Garat, C., Le Comte, E., Lee, Q.-M., Médale, J.-L., Moirin, D., Penou, E., Petiot, M., Peyre, G., Rouzaud, J., Séran, H.-C., Němeček, Z., Šafránková, J., Marcucci, M. F., Bruno, R., Consolini, G., Miyake, W., Shinohara, I., Hasegawa, H., Seki, K., Coates, A. J., Leblanc, F., Verdeil, C., Katra, B., Fontaine, D., Illiano, J.-M., Berthelier, J.-J., Techer, J.-D., Fraenz, M., Fischer, H., Krupp, N., Woch, J., Bührke, U., Fiethe, B., Michalik, H., Matsumoto, H., Yanagimachi, T., Miyoshi, Y., Mitani, T., Shimoyama, M., Zong, Q., Wurz, P., Andersson, H., Karlsson, S., Holmström, M., Kazama, Y., Ip, W.-H., Hoshino, M., Fujimoto, M., Terada, N., Keika, K., and BepiColombo Mio, M. T.: Pre-flight Calibration and Near-Earth Commissioning Results of the Mercury Plasma Particle Experiment (MPPE) Onboard MMO (Mio), Space Sci Rev, 217, 70, 10.1007/s11214-021-00839-2, 2021.

Saunders, M. A., Russell, C. T., and Sckopke, N.: Flux transfer events: Scale size and interior structure, Geophys Res Lett, 11, 131-134, 10.1029/GL011i002p00131, 1984.

Sauvaud, J. A., Fedorov, A., Aoustin, C., Seran, H. C., Le Comte, E., Petiot, M., Rouzaud, J., Saito, Y., Dandouras, J., Jacquey, C., Louarn, P., Mazelle, C., and Médale, J. L.: The Mercury Electron Analyzers for the Bepi Colombo mission, Adv Space Res, 46, 1139-1148, https://doi.org/10.1016/j.asr.2010.05.022, 2010.

Schindler, K., Pfirsch, D., and Wobig, H.: Stability of two-dimensional collision-free plasmas, Plasma Phys, 15, 1165-1184, 10.1088/0032-1028/15/12/001, 1973.

Shi, Q. Q., Zong, Q. G., Zhang, H., Pu, Z. Y., Fu, S. Y., Xie, L., Wang, Y. F., Chen, Y., Li, L., Xia, L. D., Liu, Z. X., Fazakerley, A. N., Reme, H., and Lucek, E.: Cluster observations of the entry layer equatorward of the cusp under northward interplanetary magnetic field, J Geophys Res Space Phys, 114, 10.1029/2009JA014475, 2009.

Shi, Q. Q., Zong, Q. G., Fu, S. Y., Dunlop, M. W., Pu, Z. Y., Parks, G. K., Wei, Y., Li, W. H., Zhang, H., Nowada, M., Wang, Y. B., Sun, W. J., Xiao, T., Reme, H., Carr, C., Fazakerley, A. N., and Lucek, E.: Solar wind entry into the high-latitude terrestrial magnetosphere during geomagnetically quiet times, Nat Commun, 4, 1466, 10.1038/ncomms2476, 2013.

Slavin, J. A., Imber, S. M., Boardsen, S. A., DiBraccio, G. A., Sundberg, T., Sarantos, M., Nieves-Chinchilla, T., Szabo, A., Anderson, B. J., Korth, H., Zurbuchen, T. H., Raines, J. M., Johnson, C. L., Winslow, R. M., Killen, R. M., McNutt Jr., R. L., and Solomon, S. C.: MESSENGER observations of a flux-transfer-event shower at Mercury, J Geophys Res Space Phys, 117, 10.1029/2012ja017926, 2012.

Slavin, J. A., Lepping, R. P., Wu, C.-C., Anderson, B. J., Baker, D. N., Benna, M., Boardsen, S. A., Killen, R. M., Korth, H., Krimigis, S. M., McClintock, W. E., McNutt Jr., R. L., Sarantos, M., Schriver, D., Solomon, S. C., Trávníček, P., and Zurbuchen, T. H.: MESSENGER observations of large flux transfer events at Mercury, Geophys Res Lett, 37, 10.1029/2009gl041485, 2010.

Slavin, J. A., Acuña, M. H., Anderson, B. J., Baker, D. N., Benna, M., Boardsen, S. A., Gloeckler, G., Gold, R. E., Ho, G. C., Korth, H., Krimigis, S. M., McNutt, R. L., Raines, J. M., Sarantos, M., Schriver, D., Solomon, S. C., Trávníček, P., and Zurbuchen, T. H.: MESSENGER Observations of Magnetic Reconnection in Mercury's Magnetosphere, Science, 324, 606, 10.1126/science.1172011, 2009.

Song, P. and Russell, C. T.: Model of the formation of the low-latitude boundary layer for strongly northward interplanetary magnetic field, J Geophys Res Space Phys, 97, 1411-1420, https://doi.org/10.1029/91JA02377, 1992.

Sonnerup, B. U. Ö.: Magnetopause reconnection rate, J Geohys Res, 79, 1546-1549, 10.1029/JA079i010p01546, 1974.

Sonnerup, B. U. Ö. and Cahill Jr., L. J.: Magnetopause structure and attitude from Explorer 12 observations, J Geohys Res, 72, 171-183, 10.1029/JZ072i001p00171, 1967.

Sonnerup, B. U. Ö. and Scheible, M.: Minimum and maximum variance analysis, in: Analysis methods for multi-spacecraft data, edited by: Paschmann, G., and Daly, P. W., ESA Publication, Noordwijk, Netherlands., 185-220, 1998.

Sonnerup, B. U. Ö., Paschmann, G., Papamastorakis, I., Sckopke, N., Haerendel, G., Bame, S. J., Asbridge, J. R., Gosling, J. T., and Russell, C. T.: Evidence for magnetic field reconnection at the Earth's magnetopause, J Geophys Res Space Phys, 86, 10049-10067, 10.1029/JA086iA12p10049, 1981.

Stawarz, J. E., Eastwood, J. P., Phan, T. D., Gingell, I. L., Shay, M. A., Burch, J. L., Ergun, R. E., Giles, B. L., Gershman, D. J., Contel, O. L., Lindqvist, P. A., Russell, C. T., Strangeway, R. J., Torbert, R. B., Argall, M. R., Fischer, D., Magnes, W., and Franci, L.: Properties of the Turbulence Associated with Electron-only Magnetic Reconnection in Earth's Magnetosheath, Astrophys J, 877, L37, 10.3847/2041-8213/ab21c8, 2019.

Sun, W., Dewey, R. M., Aizawa, S., Huang, J., Slavin, J. A., Fu, S., Wei, Y., and Bowers, C. F.: Review of Mercury's dynamic magnetosphere: Post-MESSENGER era and comparative magnetospheres, Sci China Earth Sci, 65, 25-74, 10.1007/s11430-021-9828-0, 2022.

Sun, W. J., Slavin, J. A., Smith, A. W., Dewey, R. M., Poh, G. K., Jia, X., Raines, J. M., Livi, S., Saito, Y., Gershman, D. J., DiBraccio, G. A., Imber, S. M., Guo, J. P., Fu, S. Y., Zong, Q. G., and Zhao, J. T.: Flux Transfer Event Showers at Mercury: Dependence on Plasma β and Magnetic Shear and Their Contribution to the Dungey Cycle, Geophys Res Lett, 47, e2020GL089784, https://doi.org/10.1029/2020GL089784, 2020.

Tang, B. B., Wang, C., and Li, W. Y.: The magnetosphere under the radial interplanetary magnetic field: A numerical study, J Geophys Res Space Phys, 118, 7674-7682, https://doi.org/10.1002/2013JA019155, 2013.

Toledo-Redondo , S., Hwang , K.-J., Escoubet , C. P., Lavraud , B., Fornieles , J., Aunai , N., Fear , R. C., Dargent , J., Fu, H. S., Fuselier , S. A., Genestreti , K. J., Khotyaintsev , Y. V., Li, W. Y., Norgren , C., and Phan , T. D.: Solar Wind—Magnetosphere Coupling During Radial Interplanetary Magnetic Field Conditions: Simultaneous Multi-Point Observations, J Geophys Res Space Phys, 126, e2021JA029506, https://doi.org/10.1029/2021JA029506, 2021.

Trattner, K. J., Mulcock, J. S., Petrinec, S. M., and Fuselier, S. A.: Probing the boundary between antiparallel and component reconnection during southward interplanetary magnetic field conditions, J Geophys Res Space Phys, 112, https://doi.org/10.1029/2007JA012270, 2007.

Trattner, K. J., Petrinec, S. M., Fuselier, S. A., and Phan, T. D.: The location of reconnection at the magnetopause: Testing the maximum magnetic shear model with THEMIS observations, J Geophys Res Space Phys, 117, https://doi.org/10.1029/2011JA016959, 2012.

Trattner, K. J., Fuselier, S. A., Petrinec, S. M., Burch, J. L., Ergun, R., and Grimes, E. W.: Long and Active Magnetopause Reconnection X-Lines During Changing IMF Conditions, J Geophys Res Space Phys, 126, e2020JA028926, https://doi.org/10.1029/2020JA028926, 2021.

Trattner, K. J., Burch, J. L., Ergun, R., Eriksson, S., Fuselier, S. A., Giles, B. L., Gomez, R. G., Grimes, E. W., Lewis, W. S., Mauk, B., Petrinec, S. M., Russell, C. T., Strangeway, R. J., Trenchi, L., and Wilder, F. D.: The MMS Dayside Magnetic Reconnection Locations During Phase 1 and Their Relation to the Predictions of the Maximum Magnetic Shear Model, J Geophys Res Space Phys, 122, 11,991-912,005, https://doi.org/10.1002/2017JA024488, 2017.

Walker, R. J. and Russell, C. T.: Flux transfer events at the Jovian magnetopause, J Geophys Res Space Phys, 90, 7397-7404, 10.1029/JA090iA08p07397, 1985.

Wang, Y. L., Elphic, R. C., Lavraud, B., Taylor, M. G. G. T., Birn, J., Russell, C. T., Raeder, J., Kawano, H., and Zhang, X. X.: Dependence of flux transfer events on solar wind conditions from 3 years of Cluster observations, J Geophys Res Space Phys, 111, doi:10.1029/2005JA011342, 2006.

Wang, Y. L., Elphic, R. C., Lavraud, B., Taylor, M. G. G. T., Birn, J., Raeder, J., Russell, C. T., Kawano, H., Zong, Q.-G., Zhang, H., Zhang, X. X., and Friedel, R. H.: Initial results of high-latitude magnetopause and low-latitude flank flux transfer events from 3 years of Cluster observations, J Geophys Res Space Phys, 110, doi:10.1029/2005JA011150, 2005.

Zhang, H., Khurana, K. K., Kivelson, M. G., Angelopoulos, V., Pu, Z. Y., Zong, Q.-G., Liu, J., and Zhou, X.-Z.: Modeling a force-free flux transfer event probed by multiple Time History of Events and Macroscale Interactions during Substorms (THEMIS) spacecraft, J Geophys Res Space Phys, 113, 10.1029/2008ja013451, 2008.

Zhao, J. T., Sun, W.-J., Zong, Q. G., Slavin, J. A., Zhou, X. Z., Dewey, R. M., Poh, G. K., and Raines, J. M.: A Statistical Study of the Force Balance and Structure in the Flux Ropes in Mercury's Magnetotail, J Geophys Res Space Phys, 124, 5143-5157, 10.1029/2018ja026329, 2019.

Zhou, M., Berchem, J., Walker, R. J., El-Alaoui, M., Deng, X., Cazzola, E., Lapenta, G., Goldstein, M. L., Paterson, W. R., Pang, Y., Ergun, R. E., Lavraud, B., Liang, H., Russell, C. T., Strangeway, R. J., Zhao, C., Giles, B. L., Pollock, C. J., Lindqvist, P. A., Marklund, G., Wilder, F. D., Khotyaintsev, Y. V., Torbert, R. B., and Burch, J. L.: Coalescence of Macroscopic Flux Ropes at the Subsolar Magnetopause: Magnetospheric Multiscale Observations, Phys Rev Lett, 119, 055101, 10.1103/PhysRevLett.119.055101, 2017.

Figures and Tables

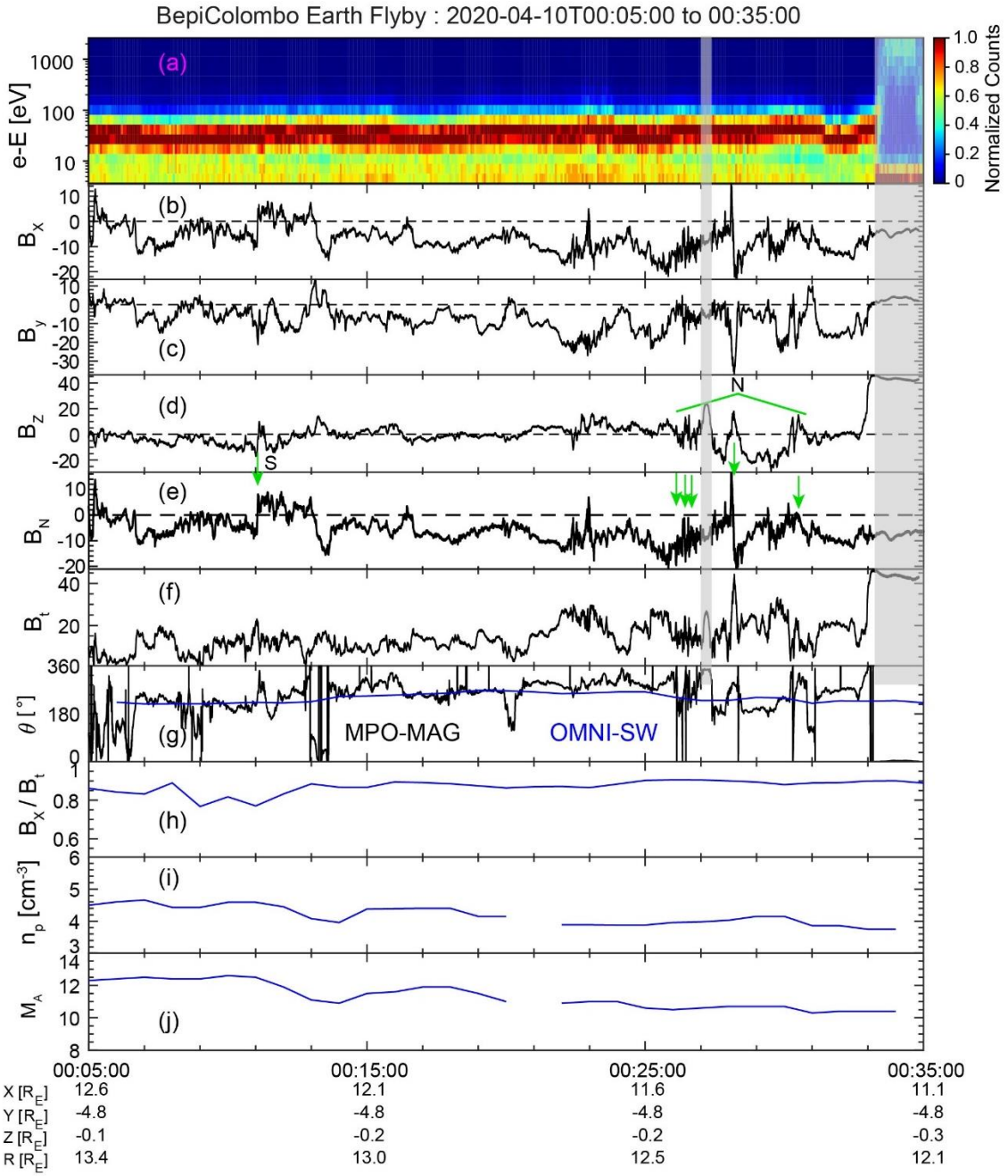

Figure 1. The electrons and magnetic field measurements of the dayside magnetopause. (a) the time-energy spectrogram of normalized electron counts from Mio/MEA, (b) magnetic x component B_x, (c) B_y, (d), B_z, (e) the magnetic component normal to the magnetopause B_N, (f) the magnetic field intensity, B_t, (g) the clock angle (θ), solar wind ratio of B_x/B_t (h), number density (n_p) (i), Alfvénic Mach number (M_A) (j). The black lines are from MPO/MAG, and the blue lines are from the OMNI. All quantities are in the Geocentric Solar Magnetospheric (GSM) coordinate. The θ in (f) is defined as arctan(B_y/B_z), ranging from 0° to 360°. The green arrows in (e) indicate the six FTE-type flux ropes. "S" indicates southward traveling and "N" northward traveling.

Table 1. List and properties of FTE-type flux ropes observed during BepiColombo's dayside magnetopause crossing

#	Time	Duration (s)	Travelling Direction	Core Field Intensity (nT)	Scale (km) [b]	Flux Content (kWb)	X^2
1	00:11:04	~ 12	Southward	— [a]	—	—	—
2	00:26:06	~ 7	Northward	~23.9	462, 388 (0.84)	~13.7	~0.04
3	00:26:26	~ 6	Northward	~60.8	565, 524 (0.93)	~22.5	~0.04
4	00:26:35	~ 4	Northward	—	—	—	—
5	00:28:13	~ 20	Northward	~41	1745, 1281 (0.73)	~300	~0.08
6	00:30:26	~ 15	Northward	~45.2	1853,1745 (0.94)	~188	~0.08

[a] "—" indicate that the values are not determined by the flux rope model. See the text for more information on the flux rope modeling.

[b] Scale contains semi-minor, semi-major, and the ratio between semi-minor and semi-major refers to the flattened profile. See the text for more information.

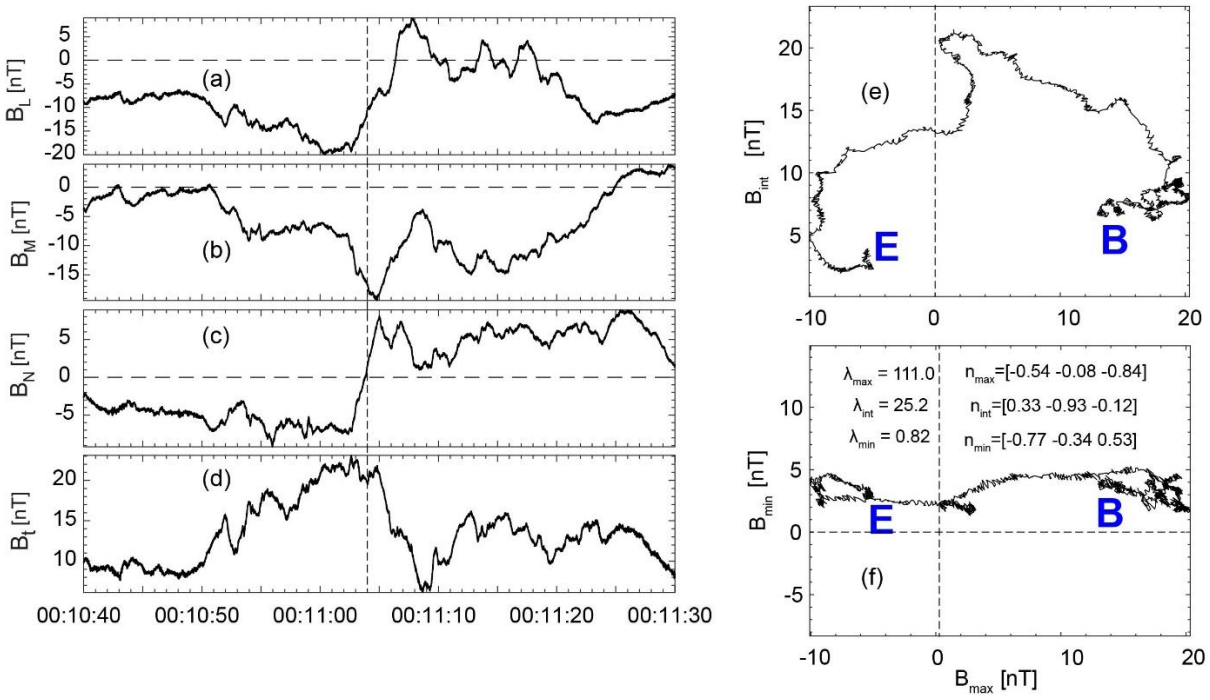

Figure 2. The southward traveling FTE-type flux rope centered at ~ 00:11:04 UT. (a) B_L, (b) B_M, (c) B_N, (d) B_t. This LMN is the local coordinate of the magnetopause. (e) and (f) are the hodograms of the magnetic field measurements under the local coordinate of the flux rope. The "B" and "E" indicate the beginning and the end of the data points.

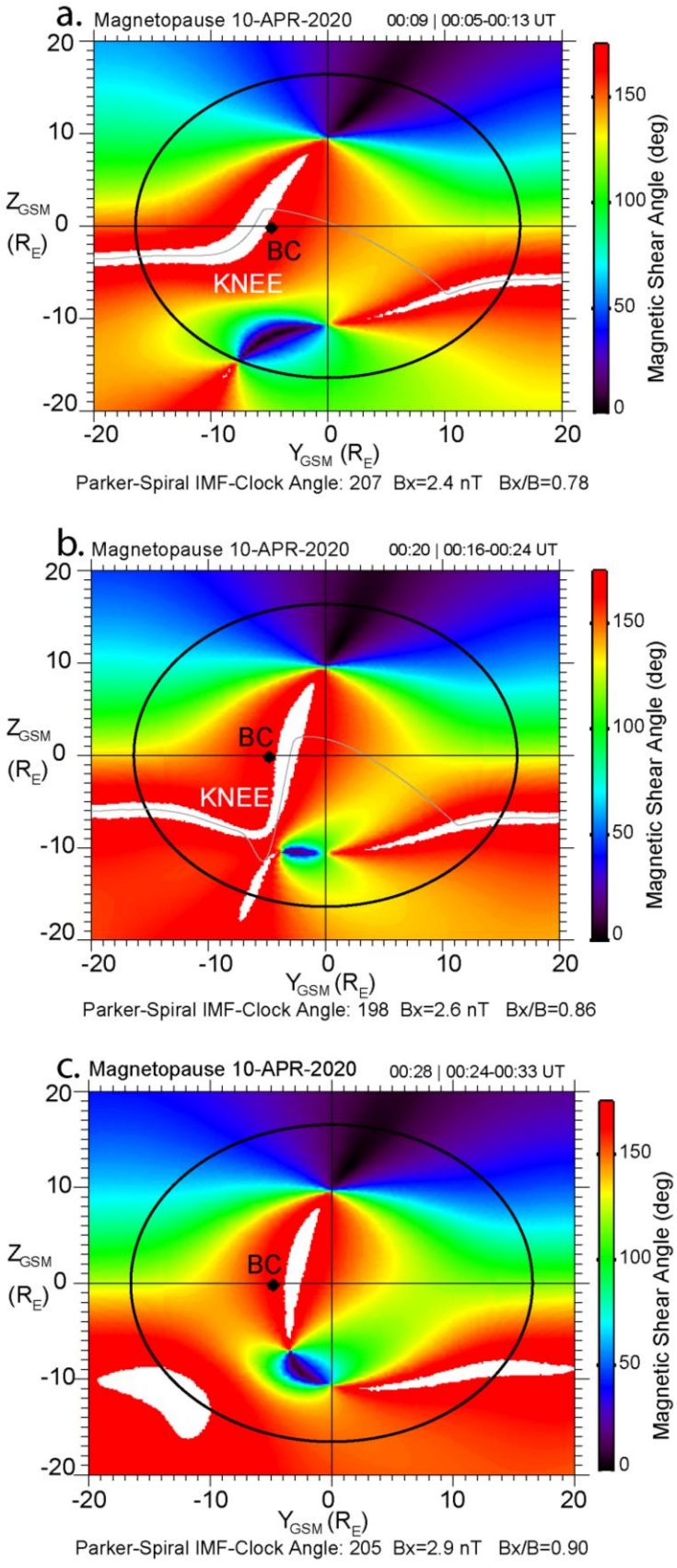

Figure 3. Magnetic shear angle plots on the magnetopause surface during BepiColombo's dayside magnetopause crossing, which are obtained through the maximum magnetic shear model [*Trattner et al.*, 2007]. (a), (b), (c) correspond to the IMF averaged from 00:05 to 00:13 UT, 00:16 to 00:24 UT and 00:24 to 00:33 UT, respectively. The black circle is the terminator plane separating the dayside magnetopause from the tailward magnetopause. The grey line is the predicted magnetopause reconnection line. White areas correspond to the magnetic shear angle is within 3° of 180°. The black dots are the location of BepiColombo ("BC"). The anti-parallel reconnection region shows a shape that is termed the "KNEE" event as it resembles a bent knee similar to an event discussed in *Trattner et al.* [2021].

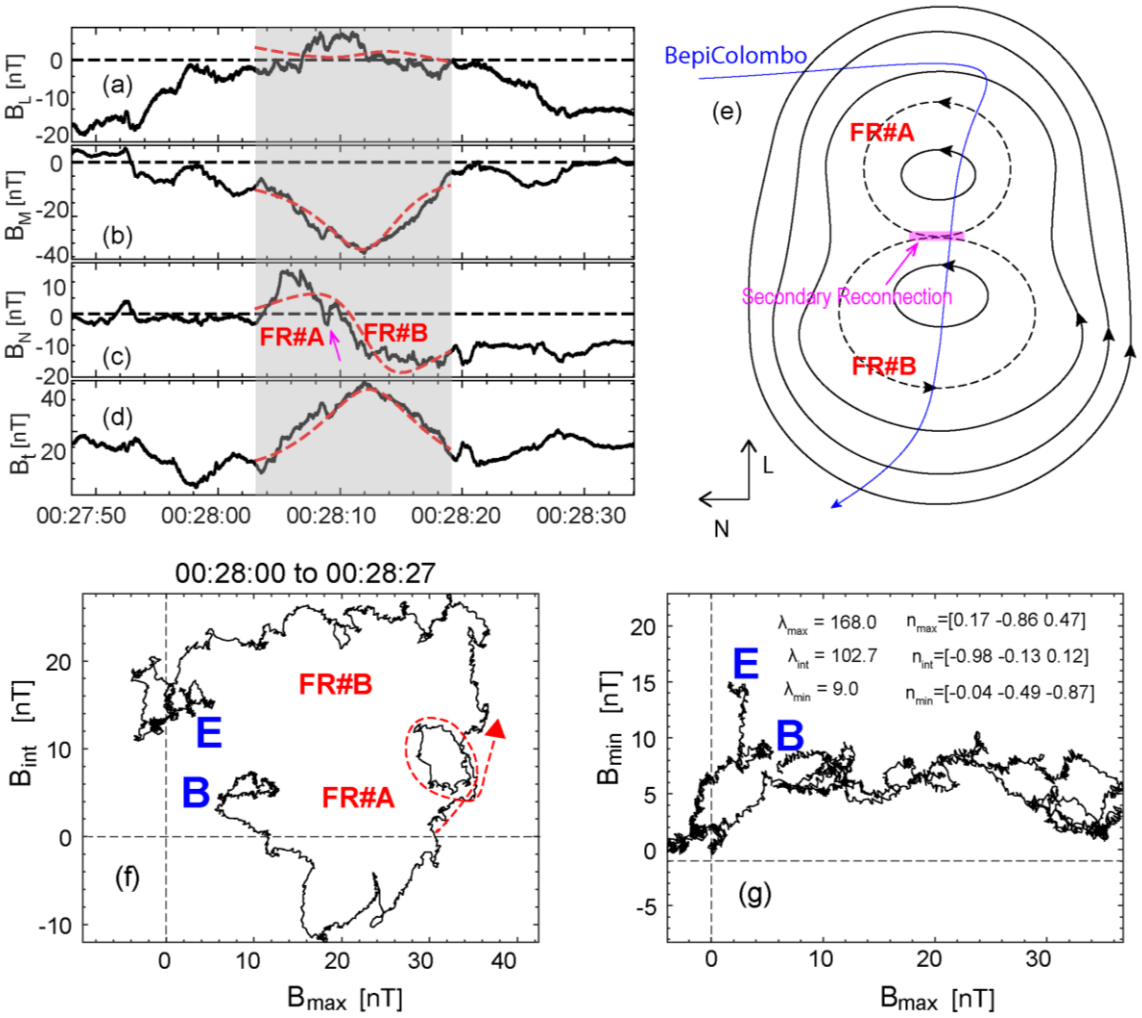

Figure 4. Overview of the flux rope centered at ~ 00:28:13 UT with the coalescence feature. (a) B_L, (b) B_M, (c) B_N, (d) B_t. The dashed lines are obtained from the flux rope model. This LMN is the local coordinate of the magnetopause. See the text for more information. (e) An illustration of the coalescence event and the BepiColombo's trajectory. The secondary reconnection site is marked by the magenta region in (e). (f) and (g) are the hodograms of the magnetic field measurements under the local coordinate of the flux rope. The "B" and "E" indicate the beginning and the end of the data points. FR#A and FR#B are the two smaller flux ropes.

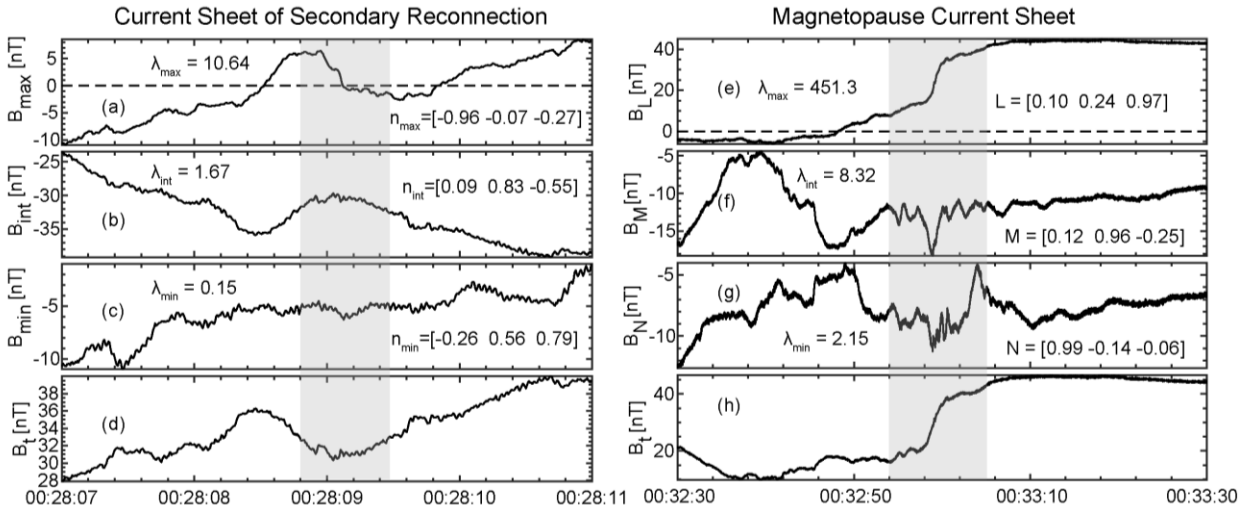

Figure 5. The magnetic field measurements under their separately local coordinate for the reconnecting current sheet of the coalescence event and the magnetopause current sheet. (a) to (d) are for the coalescence event, (e) to (h) are for the magnetopause current sheet. The eigenvalues and corresponding eigenvectors resulted from the MVA are shown.